Journal of the European Ceramic Society 20 (2000) 1–13

TEM structure of $(PyC/SiC)_n$ multilayered interphases in SiC/SiC composites

S. Bertrand*, C. Droillard, R. Pailler, X. Bourrat, R. Naslain

Laboratoire des Composites Thermostructuraux, UMR 5801 CNRS-SEP/SNECMA-UB1, Université Bordeaux, 1–3 allée de la Boétie, 33 600 Pessac, France

Received 28 January 1999; accepted 14 March 1999

Abstract

Two generations of multilayered interphases, composed of carbon and silicon carbide, have been developed to act as a mechanical fuse in SiC/SiC composites with improved oxidation resistance. Pyrocarbon is an ideal interfacial material, from the mechanical point of view, whereas SiC has a good oxidation resistance. In the multilayered interphase, the carbon mechanical fuse is split into thin sublayers, each being protected against oxidation by the neighbouring SiC-based glass former layers. A first generation of multilayers as synthesised by means of isobaric-CVI with sublayers with micrometric thickness. Then, in order to push forward the concept, pressure pulsed-CVI was involved to deposit nanometric scale sublayers. In this work, transmission electron microscopy was developed to characterise the two generations of materials. The microstructure of the layers and the influence of the fibrous preforms on the structure of the layers were studied. Examinations were then performed on the loaded samples and damaging mode characterised at nanometric scale.

Keywords: Composites; Electron microscopy; Interphase; SiC; Carbon

1. Introduction

It is now well established that the mechanical behaviour of ceramic matrix composites (CMCs) with continuous fibre reinforcement depends not only on the intrinsic properties of the fibre and the matrix, but also on the fibre–matrix bonding.[1–3] To control the strength of the fibre–matrix bonding in CMCs, an additional phase referred to as the interphase is used which serves as a compliant layer between the fibre and matrix. Two main functions are devoted to the interphase: first, load transfer between matrix and reinforcement and secondly, control of the crack deflection at the interface.[4] The interphase is deposited on the fibre surface prior to the deposition of the matrix. The most commonly used interphase materials are pyrocarbon (PyC) and boron nitride (BN). However, both of them are not stable under oxidising conditions at high temperatures. New concepts have been proposed to produce interphase that have both oxidation resistance and mechanical properties required to yield tough composites.[4,5] Also, new types of interphase involving alternating thin layers of two different materials have been suggested: the laminar ceramics.[6–10]

A breakthrough was achieved by Droillard et al.[11,12] demonstrating that $(PyC/SiC)_n$ multilayered materials, in 2D woven Nicalon/SiC composites, behaves as an efficient interfacial materials, but only if their bonding to the fibre surface is reinforced. Fig. 1, published in a previous paper,[11] shows the tensile tests realised on 2D Nicalon/SiC composites with different multilayered combinations. All the materials could be grouped into two distinct families: (i) materials reinforced with untreated fibres have a weak fibre bonding and are characterised by a relatively low strength and a low toughness, whereas (ii) materials with treated fibres possess a stronger interface and are characterised by a high strength and a high toughness. As a result, when stronger interfaces were introduced, strength and toughness were increased; in the mean time more than 50% of the carbon was removed from the interfacial zone. In contrast, when the interface was weak, only the first carbon sublayer was involved in the fracture mechanism[11] and ultimate performances remained low.

* Corresponding author.

0955-2219/99/$ - see front matter
PII: S0955-2219(99)00086-2

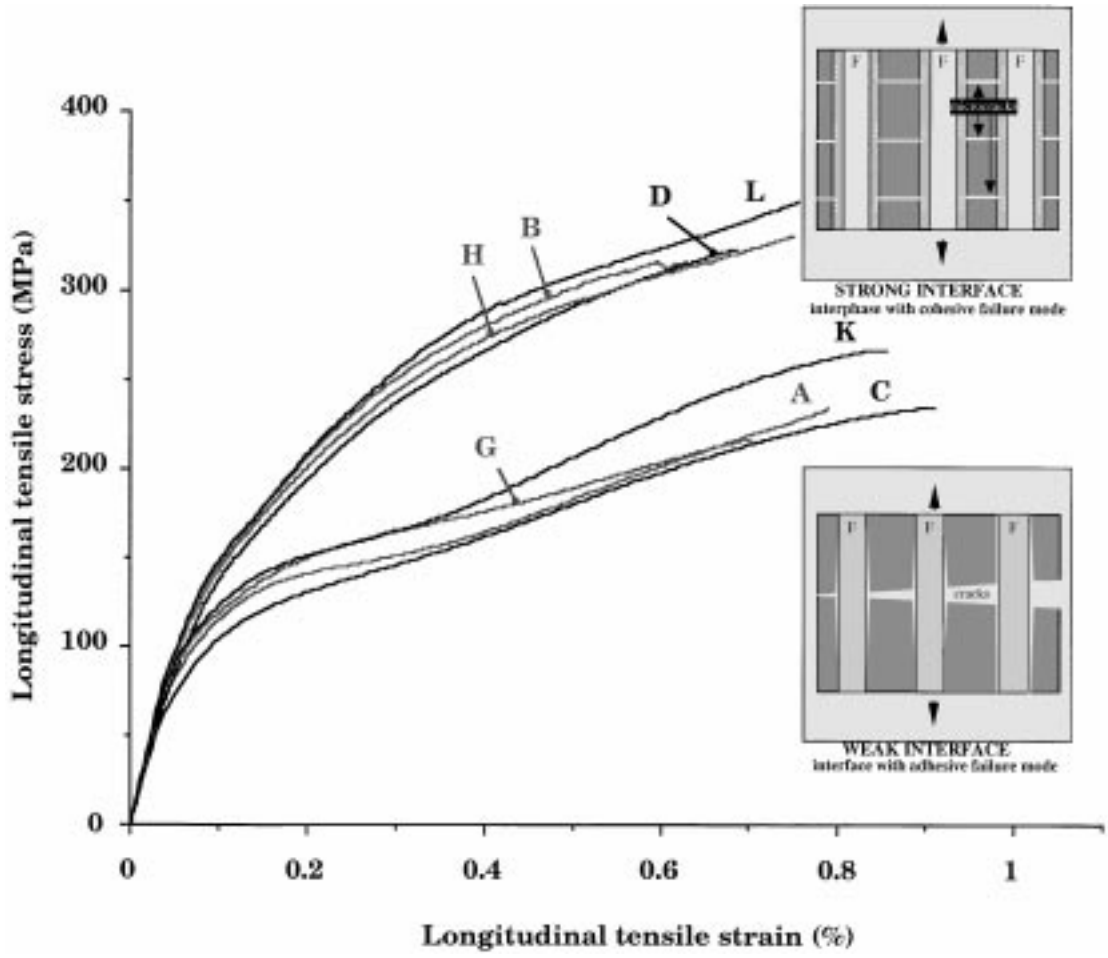

Fig. 1. Tensile stress–strain curves obtained for 2D-SiC/SiC composites with various multilayered interphases: B, D, H and L fabricated with treated Nicalon fibre; A, C, G and K fabricated with as-received Nicalon fibre (according to Refs.[4] and [11]).

Pasquier[13] has investigated the potentialities of multilayered $(PyC/SiC)_n$ interphases at the micrometer scale in Nicalon/SiC composites in terms of oxidation resistance. Then, Heurtevent[14] has developed the nanoscale multilayered $(PyC/SiC)_n$ interphases in Hi-Nicalon/SiC microcomposites and studied their behaviour at high temperatures in oxidative conditions.

The aim of the present paper is to characterise the structure of micro- and nano-scaled $(PyC/SiC)_n$ multilayered interphases. The particular aspect related to the first interface and the influence of the fibre surface treatment is fully described in a companion paper.[15]

2. Experimental procedure

2.1. 2D-SiC/SiC materials obtained by I-CVI

The 2D-SiC/SiC composites were prepared as rectangular plates ($130\times100\times5$ mm^3) from 2D-preforms consisting of stacks of Nicalon fabrics (NLM 202 ceramic grade from Nippon Carbon Company Ltd., Tokyo, Japan) maintained pressed together with a graphite tooling. The components of the multilayered $(PyC/SiC)_n$ interphases and the SiC-matrix were infiltrated within the porous fibre preforms, according to the isothermal/isobaric chemical vapour infiltration (I-CVI) process, which has been described elsewhere.[16–18] Pyrocarbon and silicon carbide were deposited from propane C_3H_8 and methyltrichlorosilane (MTS) CH_3SiCl_3/H_2, respectively, according to the following overall equations:

$$CH_3SiC_{3(g)} \xrightarrow{H_2} SiC_{(s)} + 3HCl_{(g)} \quad (1)$$

$$C_3H_{8(g)} \rightarrow 3C_{(s)} + 4H_{2(g)} \quad (2)$$

in a hot-wall chamber (internal diameter: 130 mm; height: 250 mm) heated isothermally with a water-cooled r.f. coil (maximum temperature capability: $\approx$1500°C). The apparatus has been designed to work under reduced pressures ($0.5 < P < 10$ kPa), the total pressure being maintained at a constant value with a pressure sensor (type 127A from MKS) and a pressure regulator (type 252A from MKS). Mass flowmeters were used to measure the flowrates of the various gaseous

species: propane ($Q_{C_3H_8}$), hydrogen (Q_{H_2}) and MTS (Q_{MTS}).

MTS, being a liquid at room temperature, is evaporated in a boiler set in a drying oven and then, the $MTS_{(g)}$ is mixed with hydrogen before being injected in the infiltration chamber. The composition of the gas phase used in the infiltration of SiC is characterised by a dilution α-ratio defined as:

$$\alpha = \frac{P_{H_2}}{P_{MTS}} = \frac{Q_{H_2}}{Q_{MTS}} \quad (3)$$

where P_i and Q_i (with $i = H_2$ or MTS) are the partial pressure and gas flowrate of species i, respectively. The experiments have been carried out under conditions typical of the I-CVI process, which have been discussed elsewhere.[16–18]

Two different series of 2D-SiC/SiC composites have been prepared. In the first series, the Nicalon fabrics were used as-received (materials A, C, G, and K in Table 1) whereas, in the second series (materials B, D, H, and L), the Nicalon fabrics have received a treatment (proprietary treatment performed by SEP, Bordeaux) prior to the infiltration of the multilayered interphase, in order to improve the fibre–matrix bonding.[19]

The nature of the various multilayered interphases deposited by I-CVI on the fibre surface is shown in Table 1. The interphases exhibit the following features: (i) the first sublayer (i.e. that in contact with the fibre surface) is always a pyrocarbon sublayer and the interfacial sequence can be written as $(PyC/SiC)_n$, (ii) when $n > 1$, the SiC of the last sequence is that of the matrix, (iii) the overall thickness of the multilayered interphase is constant and equal to 0.5 μm and (iv) the thicknesses of the C and SiC sublayers are either maintained constant (materials G, H) or evolutive (materials K, L) within the interphase. Finally, the thickness of the PyC sublayers has been limited to 0.1 μm or less for oxidation resistance considerations (which will be not developed here).

Table 1
Material references and nature of the multilayered interphases of the 2D Nicalon/SiC composites, processed by I-CVI

Materials	Nature of the fabrics	Nature of the C-SiC sequence in the interphase and thickness (in μm)
A	NT[a]	F[c]/C/SiC/C/M[d]
B	T[b]	0.1 0.3 0.1
C	NT	F/C/C/SiC/M
D	T	0.1 0.1 0.1 0.1 0.1
G	NT	F/C/SiC/C/SiC/C/M
H	T	0.05 0.1 0.05 0.1 0.05 0.1 0.05
K	NT	F/C/SiC/C/SiC/C/M
L	T	0.05 0.05 0.05 0.1 0.05 0.15 0.05

[a] NT: not treated.
[b] T: treated.
[c] F: fibre.
[d] M: matrix.

2.2. Pressure pulsed-CVI: nanometric scale multilayers

The nanometric scale multilayered interphases have been fabricated by pressure pulsed CVD/CVI (P-CVD/P-CVI) process. The apparatus used for the fabrication of the materials and the experimental conditions have been described in another article.[20] In this process, the operating pressure is pulsed. First, admission of reacting gas is allowed by an upper inlet pneumatic valve, up to the operating pressure. Then the furnace is closed during a residence time, t_r and, finally, it is evacuated through an outlet pneumatic valve, and cooled traps by using a rotary pump. A computer is used to monitor valves' opening and closing, safety devices and the total amount of pulses.

Hi-Nicalon bundles (from Nippon Carbon Company Ltd., Tokyo, Japan), were used for the fabrication of SiC/SiC minicomposites (a minicomposite is a model 1D composite with one single fibre tow). In order to change the interfacial bonding strength two series of reinforcement were systematically utilised: in the first series, tows were used as-received (i.e. non treated fibres) whereas, in the second series, the tows were previously submitted to a treatment (so-called treated fibres) performed at the Laboratory, prior to the infiltration (or deposition) of the multilayered interphase. The nature of the various multilayered interphase is shown in Table 2.

2.3. Microstructural characterisation

Microstructure of the multilayers was essentially assessed by Transmission Electron Microscopy (TEM, CM30ST/PEELS from Philips). TEM analyses were performed on sample cross-sections, perpendicular to the axis of the fibres as well as longitudinal sections. TEM specimen sampling has been previously detailed in a companion paper.[15]

Optical microscopy in polarised light (MeF3 from Reichert-Jung) was used to measure the pyrocarbon anisotropy following the extinction angle technique (Ae), fully described elsewhere.[21] Ae was observed to fall between 12° and 14° corresponding to smooth laminar (SL) and rough laminar (RL) pyrocarbon.

X-Ray Diffraction (XRD, Siemens D5000) analysis was performed in order to evaluate the apparent crystallite size in the [111] crystallographic direction (L_{111}) of the SiC grains by means of the Scherrer equation ($k = 0.9$).

Auger Electron Spectroscopy (AES) microprobe equipped with an Ar^+ sputtering gun (VG 310F) was used to record composition-depth profiles.

Fracture surfaces were examined by Scanning Electron Microscopy (FEG-SEM Hitachi S4500) at low voltage (3 kV).

3. Results—micrometer-scale multilayers as processed by I-CVI

When seen in cross section, multilayers deposited by means of I-CVI exhibited rough and discontinuous sublayers (Fig. 2). The inset shows a low magnification of interphase "G" constituted by seven sublayers infiltrated in an as-received 2D Nicalon NLM 202-based preform. This sequenced ceramic material appears rough and disrupted. A close inspection at higher magnification revealed that carbon sublayers were systematically continuous, and that disruptions, when present, were related to the SiC sublayer crystallinity.

Table 2
Material references and nature of the multilayered interphases of the Hi-Nicalon/SiC minicomposites, processed by P-CVI

Materials	Nature of the tows	Nature of the C-SiC sequence in the interphase and thickness (in nm)
15	NT[a]	F[c]/(PyC/SiC)$_{10}$/M[d]
54	T[b]	20 50
45	NT	F/(PyC/SiC)$_{10}$/M
		3 30

[a] NT: non treated.
[b] T: treated.
[c] F: fibre.
[d] M: matrix.

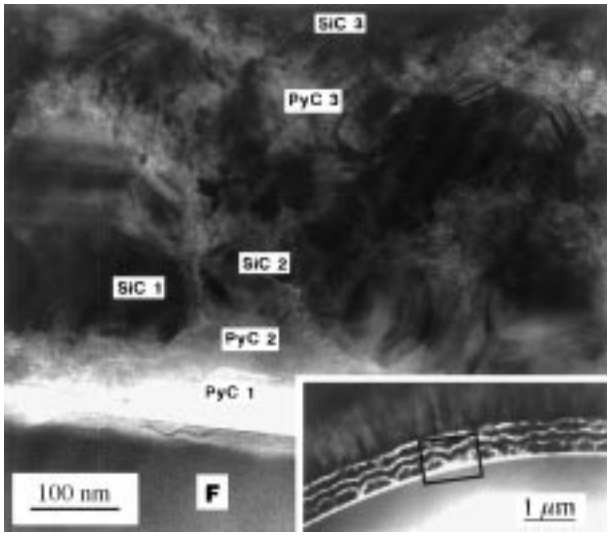

Fig. 2. Cross-section of the interfacial sequence in material G (TEM contrasted brightfield): undulation of the layers related to the crystallinity of SiC. Inset is a low magnification of an equivalent area (same technique).

3.1. Pyrocarbon nanostructure

Generally speaking, pyrocarbon resulting from the cracking of propane under the I-CVI conditions was characterised by a large value of the L_2-parameter, a strong anisotropy and a low porosity[22] (L_2 characterises the lateral size of the aromatic carbon sheet in the turbostratic stack as measured by HR-TEM). Similar features have been also reported for pyrocarbons resulting from the cracking of propylene C_3H_6.[23]

The first pyrocarbon sublayer growth occurred directly onto the fibre surface whose composition was different for the two series of materials considered here. The bonding of carbon onto the fibre was seen to control the nature of the composite interface.[15] Then, all the subsequent pyrocarbon sublayers grew onto surfaces made of pure, well crystallised SiC which exhibited some roughness at the nanometric scale. As shown in Fig. 3, the PyC deposit first filled the concave parts (formed by adjacent cone-like SiC crystals) of the SiC-substrate. Then, at a distance, the PyC aromatic layers tended to deposit parallel to the mean surface of the coated fibre and exhibited a pronounced anisotropy. The analysis of the first carbon layers has not shown (on the basis of the TEM images) any significant difference in the carbon organisation depending on the nature of the sublying SiC crystals.

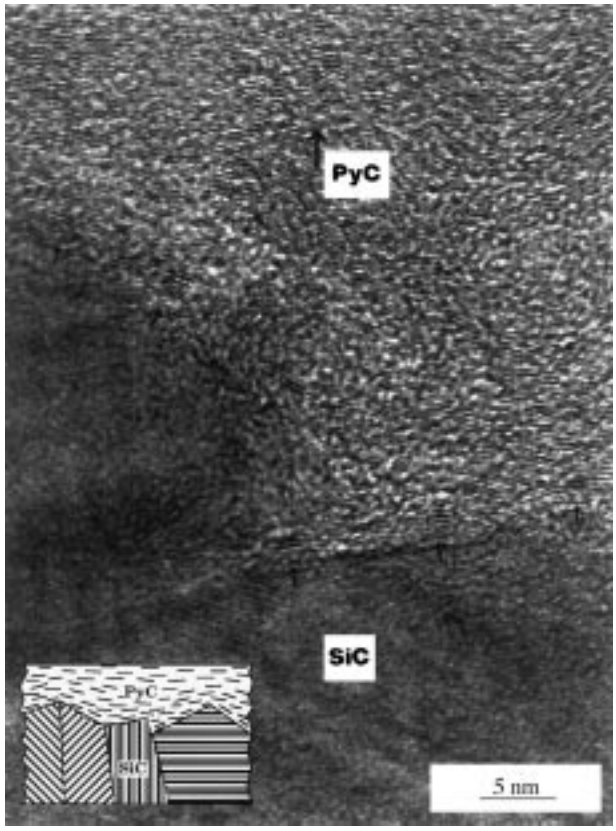

Fig. 3. Growth of the first pyrocarbon layers onto a well crystallised SiC surface: smoothing effect of carbon (high resolution TEM).

3.2. Nanostructure of the SiC-sublayers

The SiC present in the multilayered $(PyC/SiC)_n$ interphase was always deposited onto pyrocarbon surfaces, roughly flat, as supported by a comparison of the pyrocarbon C(002) lattice fringes TEM images (recorded at about the same magnification) shown in Figs. 3 and 4. Fig. 4 shows that there is probably some relation between the orientation of the carbon aromatic planes in the substrate and that of the crystals in the SiC-deposit. Meanwhile, no precise relationship was found for the preferred growth directions of SiC (i.e. 111 for the cubic β modification and 00.1 for the hexagonal α modification) with respect to the C aromatic planes in the substrate.

SiC in the deposits was well crystallised, the size of the crystals being often limited by the thickness of the SiC sublayer itself. The crystals are either of the cubic (3C) β modification or consisted of a sequence of disordered polytypes, as shown in Fig. 5 and already reported by several authors.[24,25] The diffraction pattern (inset in Fig. 5) shows a straining of the reciprocal nodes along the $[111]_c$ growth axis, i.e. perpendicular to the stacking fault plane.

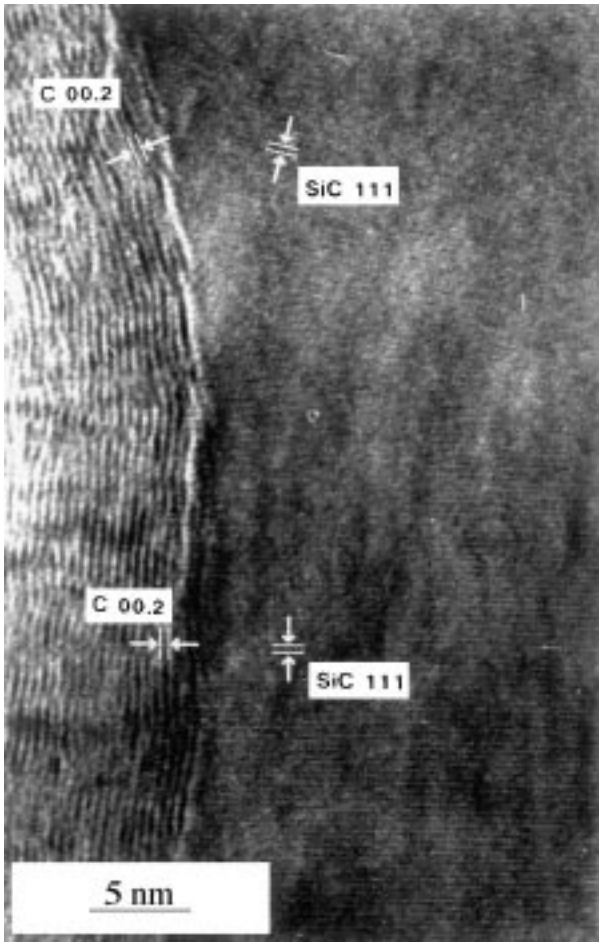

Fig. 4. Growth of SiC on the surface of PyC layer: smoothness of the interface.

The first SiC sublayer was observed to be often discontinuous, particularly when its thickness was low (i.e. 0.1 μm), as shown in Fig. 2. As a result, "mechanical bridges" were formed under such conditions, between the sublayers (inset in Fig. 2). Obviously, an optimising of the nucleation/growth processes should be further carried out in order to achieve thinner and smoother sublayers.

3.3. Multiple interfacing

The number of interfaces in the $(PyC/SiC)_n$ multilayered interphase increases as n is raised: up to 8 when $n=4$ (materials G, H, K and L) remembering that the silicon carbide in the last sequence is the matrix itself. As discussed in a previous paper,[11] the first interface has a unique role in controlling the behaviour of the whole interfacial sequence: fibre/PyC_1 bonding has to be strong in order to allow multiple deflection at the different other interfaces.[11] Fibre surface bonding strength is related to the surface state of the fibre. In addition to the first interface (fibre/PyC_1) there exists two kinds of interface characterised by a very different roughness (important features regarding debonding and friction phenomena) in such multilayered $(PyC/SiC)_n$ interphases.

The interface related to a SiC-deposit onto a PyC-layer (e.g. PyC_{n-1}/SiC_n) was usually smooth, as already mentioned, owing to the layered structure of pyrocarbon and to its "covering capability" (tending to

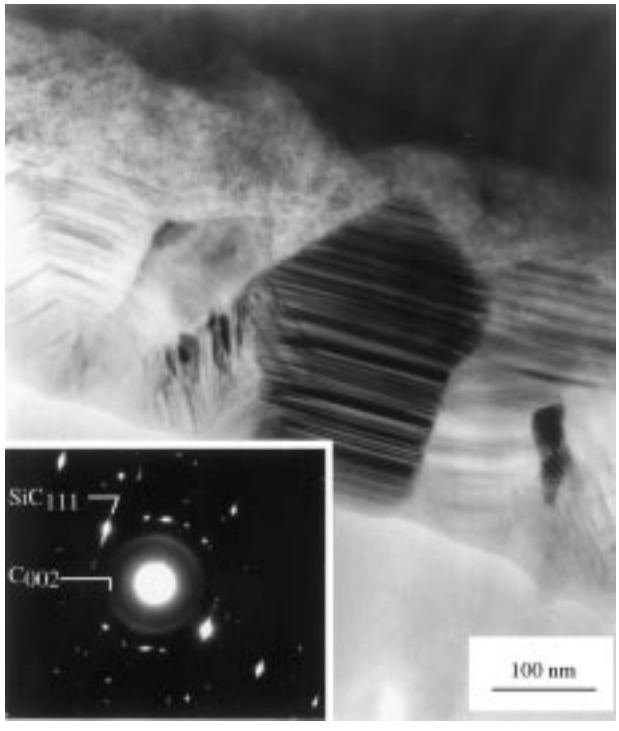

Fig. 5. Structure of the SiC-based sublayer. Inset: electron diffraction pattern centered on the contrasted crystal exhibiting one-dimensional disordered polytypism.

level the roughness of the substrate on which it has been itself deposited). Apart the fibre/PyC_1 interface obtained with the pristine fibre (which is the smoothest interface) the second interface (PyC_1/SiC_1) was systematically that with the highest smoothness whatever the nature of the material (since PyC_1 has been deposited on the fibre surface known to be smooth).

The interface related to a pyrocarbon-deposit onto a SiC-layer (e.g. SiC_{n-1}/PyC_n) exhibited a high roughness when the thickness of the SiC layer was large (owing to the tendency of SiC to grow as large-faceted crystals, as shown in Fig. 5). It can be even discontinuous when the SiC layer is very thin. Under such conditions, there occurs direct (and relatively strong) bonding between the PyC_{n-1} and PyC_n layers (Fig. 2).

3.4. Microcrack propagation path within a microscale multilayered interphase

As previously observed for single carbon interlayer,[15] matrix microcracks present in specimens loaded to failure (and especially crack-deflection-mechanisms) depend first of all on the fibre surface bonding strength (fibre/PyC_1 bonding strength). As received fibres are coated by a thin oxide layer which produces a weak bonding. In contrast, with the treated fibres, the fibre surface bonding strength is raised. The detailed analysis of the microcrack propagation paths fully supports the classification of the materials in two families previously done on the basis of the mechanical behaviour and corresponding to the use of untreated or treated fibres, whatever the nature of the interphase (number and thickness of sublayers).

3.4.1. Composites with untreated fibres

The microcrack paths exhibit two main features: (i) all the microcracks propagate up to the Nicalon fibre surface, as shown in Fig. 6 and (ii) in the 0°-fibre-bundles, there is no longer any bonding between the fibre and the interphase, i.e. the fibre is *debonded over its full length*, as shown in Fig. 7. These features occur whatever the nature of the interphase but as long as the fibres have not been treated. Finally, for this first material family, debonding and then sliding occurred mostly along the

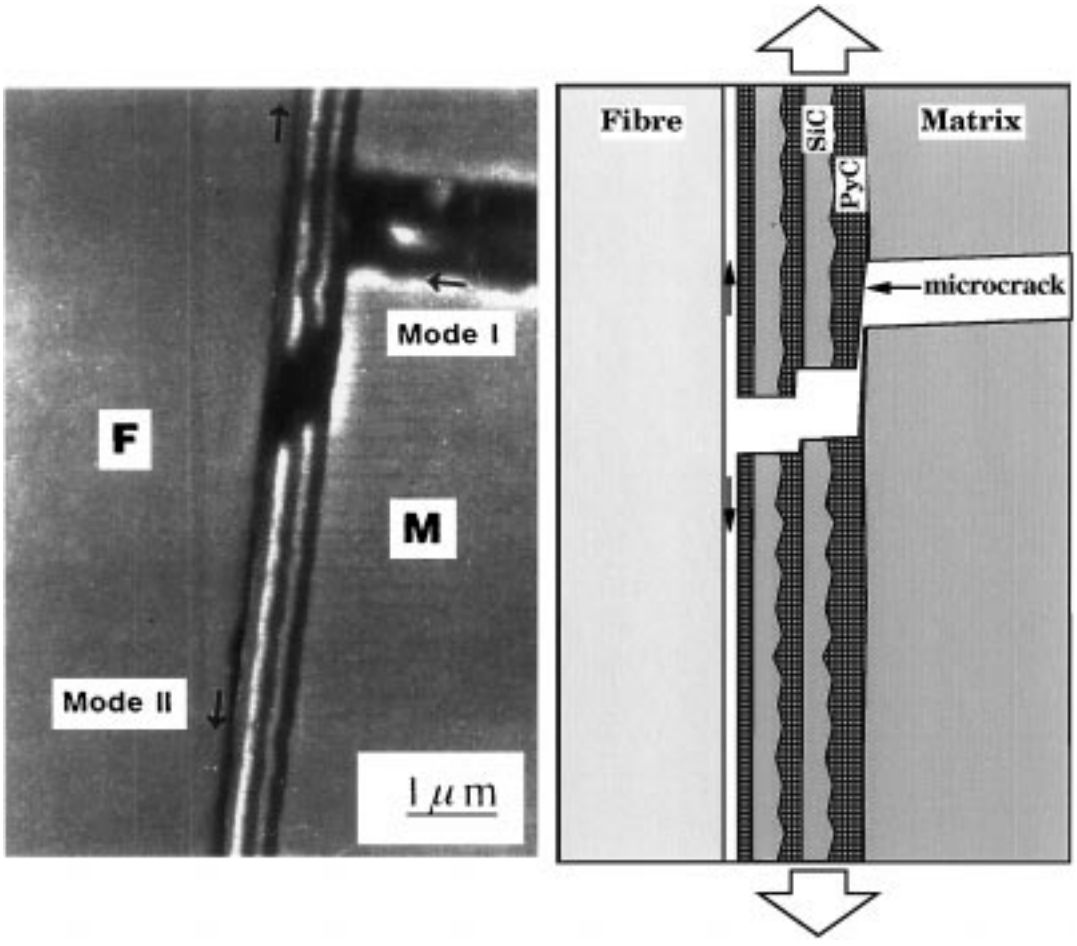

Fig. 6. Multilayered interphase (material G with untreated Nicalon fibre) loaded to failure: (a) SEM micrograph on a polished longitudinal section showing the propagation path of a matrix microcrack (arrow) deflected in mode II on fibre surface; (b) schematic showing the large residual crack opening and the final deflection at the fibre surface (open arrows indicate the loading direction).

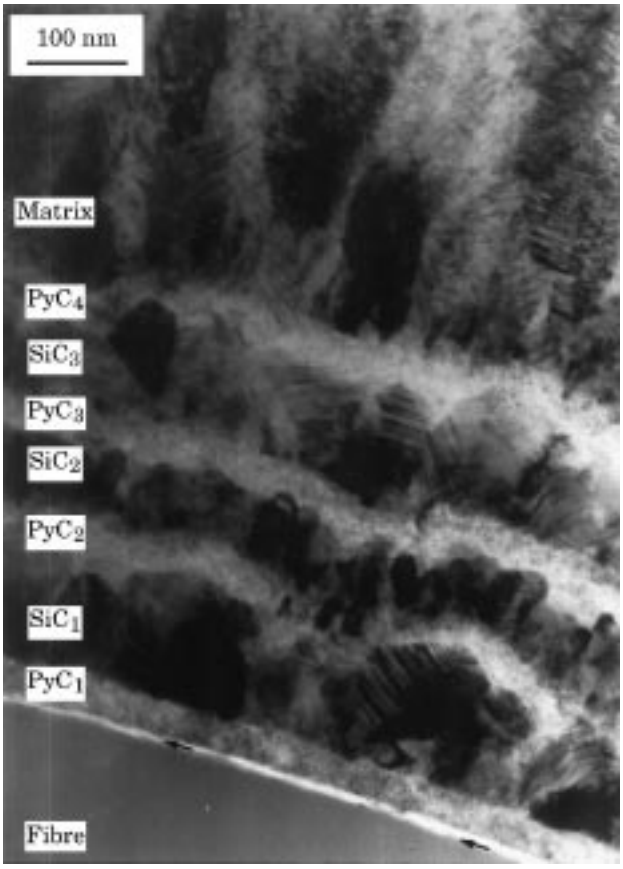

Fig. 7. Material G (untreated Nicalon fibre). TEM cross-section (after failure) showing the fibre/multilayer debonding anywhere in the material.

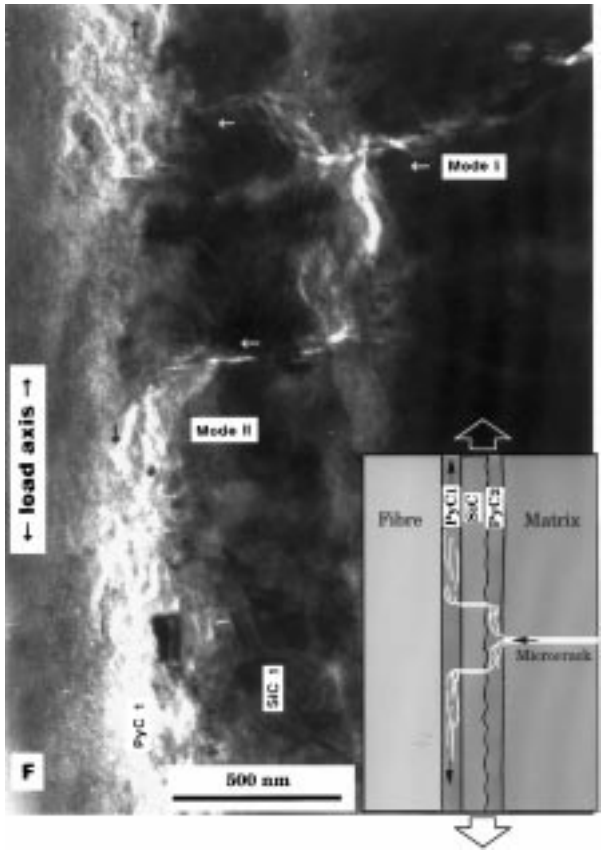

Fig. 8. Material B (treated Nicalon fibre) after failure. TEM longitudinal section exhibiting a cohesive failure mode of the multilayered interphase with multideflection (inset: schematic deflection in strong interface).

first interface which is very smooth, geometrically well defined and also very weak on a chemical view point.[15]

3.4.2. Composites with treated fibres

Matrix microcrack deflections exhibit very different features for the composites fabricated with the treated fibres. First, it was never seen any matrix microcrack propagating up to the first interface, i.e. the fibre/PyC_1 interface. The fibre remains bonded over its full length (except very near the matrix microcracks) even at the matrix crack saturation step; the fibre-matrix being never uncoupled in a net manner (as observed in the other material family). As the fibre is being strained under loading, debonding and then sliding (if there is still any) no long occur along a well geometrically defined surface but *in a diffuse manner*. Microcracks seem to burst into an infinity of nanometric-scale cracks as they are deflected in a pyrocarbon layer, parallel to the fibre-axis. This was clearly identified to a shearing failure mode in the case of a simple pyrocarbon interlayer.[15] This is illustrated for material B in Fig. 8. Deflecting within the whole thickness of the interphase (and not only as a single debonded surface) is a key feature of composites fabricated with treated Nicalon fibres, which has been already described for single pyrocarbon interphase. Owing to the high number of cracks produced during this deflection, this damaging mode appears as a highly dissipating mechanism and results in a higher toughness.[12] It has been observed either for the composite with a single thick carbon layer[11] or for those with $(PyC/SiC)_n$ multilayered interphases in which the pyrocarbon sublayers are much thinner.

The second interface (PyC_1/SiC_1) owing to its smoothness, was often observed to be the interface at (or near to) which the mode I/mode II deflection occurred, as shown in Fig. 9. The fibre is not debonded. Sometimes, microcracks were seen to be deflected at an interface of much higher order. As an example, Fig. 10 shows the case of a deflection within the last carbon sublayer, far away from the fibre (favourable for protection against oxidation).

Finally, a very common feature of the multilayer as deflector was the multideflection mode as seen for example in Fig. 8. The matrix microcrack underwent a mode I/mode II deflection and then a mode II/mode I and so on...This multideflection mode was abundantly seen in the case of the treated fibre. This is the toughening-based mechanism suspected for that class of material together with the matrix multiple cracking.

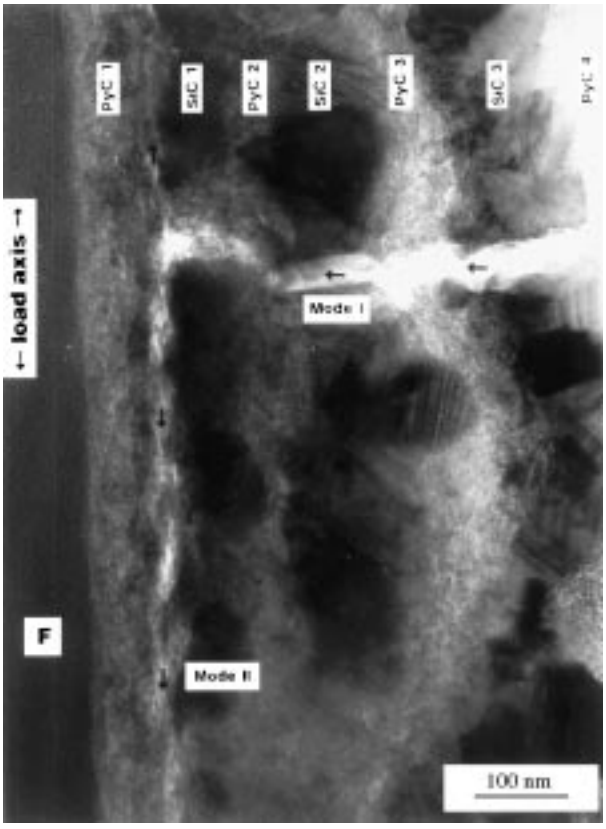

Fig. 9. Material L (treated Nicalon fibre). Mode I/mode II deflection of a matrix microcrack at the second interface. Note that the first interface (fibre/PyC_1) is not debonded (TEM brightfield, sample loaded to failure).

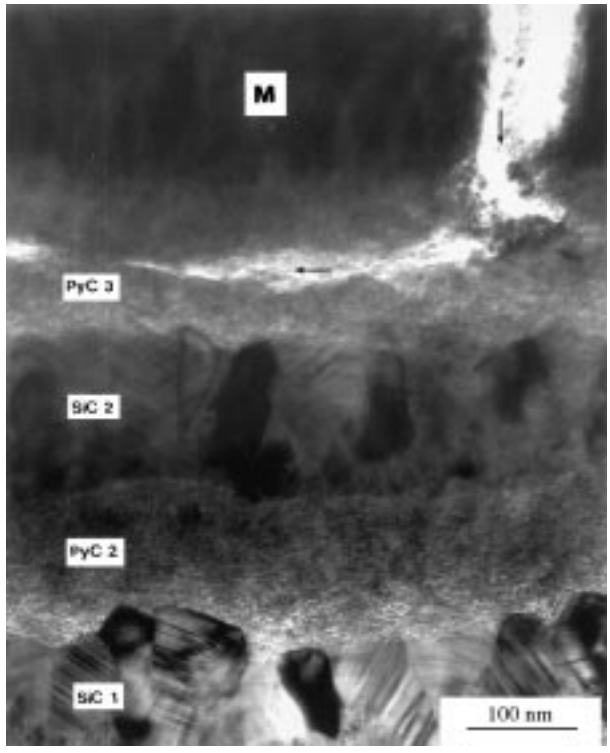

Fig. 10. Material D (treated Nicalon fibre). TEM longitudinal section along the 0° bundle showing a mode I/mode II deflection in the last interfacial carbon sublayer.

4. Results—nanometer-scale multilayers processed by P-CVI

4.1. Structure of the multilayered interphases

4.1.1. Regularity and continuity of the layers

Fig. 11(a) shows an example of a multilayered interphase processed at nanometric scale. This micrograph is a cross section in a minicomposite obtained with as-received Hi-Nicalon fibres and a multilayered interphase: $(PyC_3/SiC_{30})_{10}$ (3 and 30 being the PyC and SiC layer thicknesses in nm and 10 the number of PyC/SiC sequences in the multilayer). A higher magnification [Fig. 11(b)] shows that pyrocarbon and SiC-based sublayers are regular and continuous. The P-CVI process[14] enables to deposit thin layers, parallel to the surface of the fibres. It enables also to control the α-gaseous ratio H_2/MTS known to control the deposit composition and crystallinity (here, the SiC-based layers do not consist of pure SiC but of a nanocrystalline SiC + C mixture).[14] Sharp interfaces between hard and compliant materials are now accessible with that process. This has to be compared to those obtained at higher scale with I-CVI (Fig. 2). Layer flatness and thereafter interface sharpness are suspected to be key features for obtaining a layered material with improved toughness.

4.1.2. The fibre surface and the first interface

The first material deposited on the fibre surface is systematically a pyrocarbon layer. Results of AES depth-profile analyses, performed on the untreated and treated fibres, prior to any P-CVI infiltration, were performed in order to assess the chemical composition near the fibre surface. For the untreated fibres, a Hi-Nicalon yarn has been set in the reactor, and then heated under vacuum, in order to reproduce the conditions experienced by the fibre prior to interphase deposition.

The surface of the untreated fibre is composed of a Si-C-O mixture, 15 nm in thickness, assumed to be a SiO_2 + free-C phase mixture.[20] The silica is formed during the fibre heating under vacuum. When observed by TEM after the multilayer has been deposited, the fibre surface looks rather smooth and clean. Fig. 12 is a high resolution TEM micrograph of the first interface in a composite fabricated with untreated fibres and a $(PyC_3/SiC_{30})_{10}$ multilayer. The first pyrocarbon sublayer, composed of 7/8 carbon fringes, is lying directly on the SiC nanocrystals forming the free surface of the fibre. The oxide layer evidenced by AES is not observed after P-CVI, in the final material.

The surface of the treated Hi-Nicalon fibre is composed, essentially, of a free-C layer, approximately 50 nm-thick. Fig. 13 shows the interface of a material processed with a

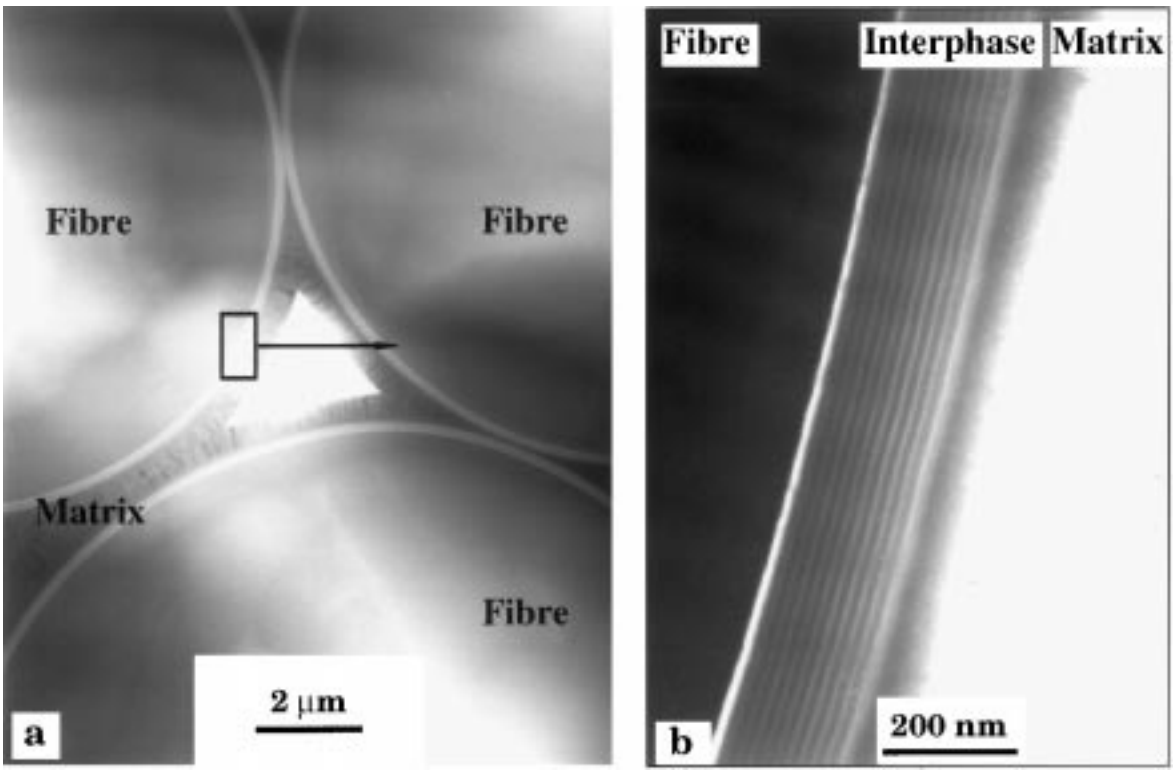

Fig. 11. TEM cross-section of a minicomposite: as-received Hi-Nicalon/$(PyC_3/SiC_{30})_{10}$/SiC. Note the sharp interfaces controlled by the poor SiC crystallisation obtained by P-CVI: (a) low magnification and (b) higher magnification on the interfacial sequence.

treated Hi-Nicalon fibre. The residual carbon layer evidenced by AES is visible but with a thickness, usually, thinner than 50 nm. It is in fact a bilayer. A rather dense carbon (less than 10 fringes) is lying directly on the surface of the fibre. Then a poorly organised carbon, at least 30 nm-thick, is observed. In Fig. 13, it can be seen than the first pyrocarbon sublayer (PyC_1) is deposited on this poorly organised carbon with a more densely packed stacking.

The two fibre surfaces are thus different, their roughness meanwhile looking equivalent. In short, depending on the occurrence of a pretreatment or not, the first interface is either a SiC/PyC_1 interface or a free-C/PyC_1 interface.

4.1.3. Nanostructure of the PyC sublayers

The nanostructure of the PyC-sublayers has been studied by TEM and optical microscopy. Values of the extinction angle (Ae),[21] obtained for the PyC deposited by P-CVI, were all around 18–19°. Each PyC sublayer grows onto surfaces made of well nanocrystallised SiC + C which exhibit some roughness at the nm-scale (excepted for the first sublayer). As shown in Figs. 12 and 13, the PyC first fills the concave parts of the SiC-based substrate, at a distance, the PyC aromatic layers tend to deposit parallel to the mean surface of the coated fibre and exhibit a pronounced anisotropy.

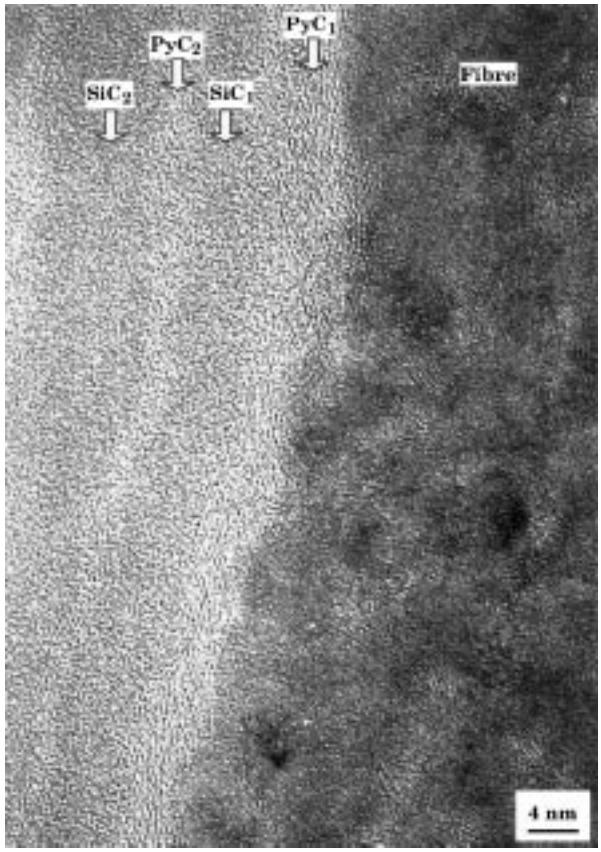

Fig. 12. Interface of an untreated Hi-Nicalon fibre reinforced SiC composite, with a $(PyC_3/SiC_{30})_{10}$ interphase.

4.1.4. Nanostructure of the SiC-based sublayers

XRD analyses have been performed on planar deposits (i.e. $(PyC/SiC)_n$ multilayer deposited by P-CVD). They show the coexistence of α and β SiC varieties as previously reported by Heurtevent.[14] The measurement of the L_{111} from the spectra, is 18.8 nm. Microanalyses, by electron probe micro-analysis (EPMA), have shown that the SiC-based sublayers, are in fact, C + SiC codeposits, as previously mentioned.[20]

In microcomposites,[14] the nanostructure of the SiC-based sublayers changes according to the thickness of the layer. Over 30 nm, a slight columnar microstructure is apparent. The first SiC-based deposit (when $e_{(SiC)} < 30$ nm) is nanocrystallised, while, beyond 30 nm, a microcrystallised layer is superimposed on this first amorphous layer.

In minicomposites, the nanostructure of the SiC-based layers changes with the distance from the fibre. The first layers are nanocrystallised, while the layers, near the matrix, are microcrystallised.

4.1.5. The interfaces

The multilayered structure is developed to multiply the number of interfaces in order to increase the work of fracture. The first interface remains meanwhile the most important which controls the whole interphase behaviour.[11] Fig. 14 compares the brightfield and the carbon 002 dark field images of the same interphase. The latter is obtained, as shown in the diffraction pattern, by selecting the information carried by the 002 reflection by means of an aperture. By this technique, only the carbon is in contrast. Despite their smooth aspect, this projection evidences the roughness of the sublayers. The multiple deflection is therefore expected to be limited.

4.2. Crack propagation in the interphase

These multilayered $(PyC/SiC)_n$ thin films have been utilised as interphase in SiC/SiC composites. Uniaxial tension tests were performed at room temperature on the micro-, mini- and 2D-composites.[14,20] After failure, the materials were studied by TEM and SEM to characterise the deflection mode and the interfacial behaviour.

The matrix microcrack deflection mode depends on the treatment of the Hi-Nicalon fibre.

When the fibre is not treated, a strong radial shrinkage occurs during the CVI processing at high temperature.[25] TEM low magnification images show clearly that a debonding occurs on most of the interfaces (arrows in Fig. 15). Even if the chemical interfacial bonding is strong, the strong fibre contraction when observed produces a high amount of debonding. As a

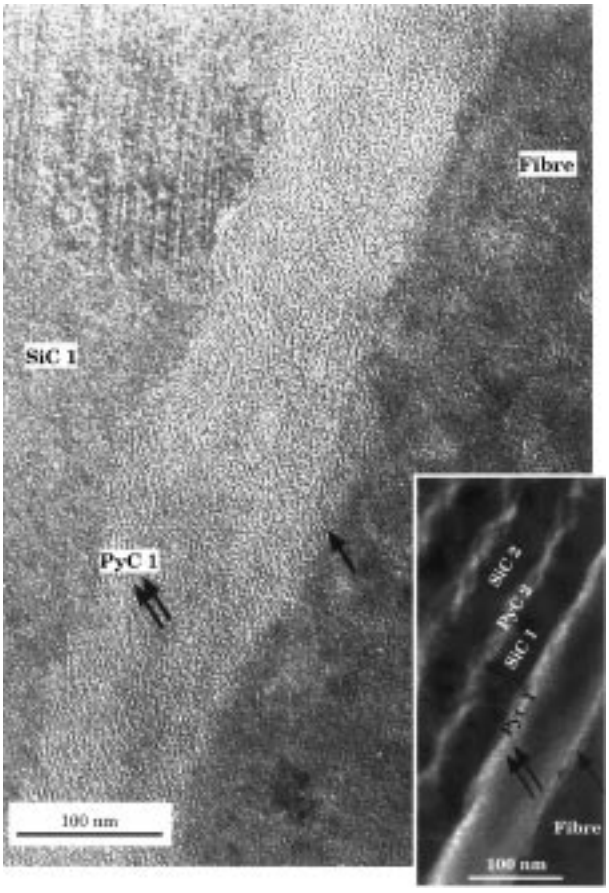

Fig. 13. Interfaces in treated Hi-Nicalon fibre-reinforced SiC composite. Inset is a 002 darkfield of the same interface showing three carbon layers at the treated Hi-Nicalon/$(PyC_{20}/SiC_{50})_{10}$ interface.

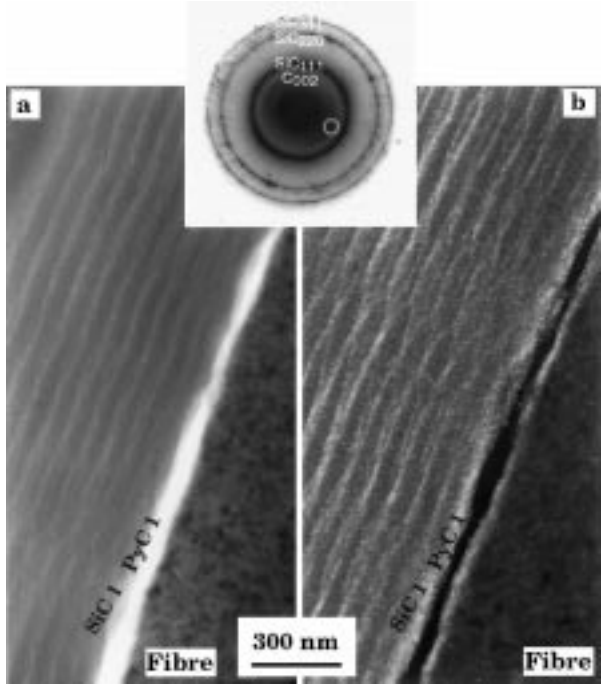

Fig. 14. Interphase $(PyC_{20}/SiC_{50})_{10}$ in a minicomposite with treated Hi-Nicalon fibres: (a) brightfield TEM image and (b) carbon 002-dark field. Inset is the electron diffraction pattern of the multilayer with the objective aperture position.

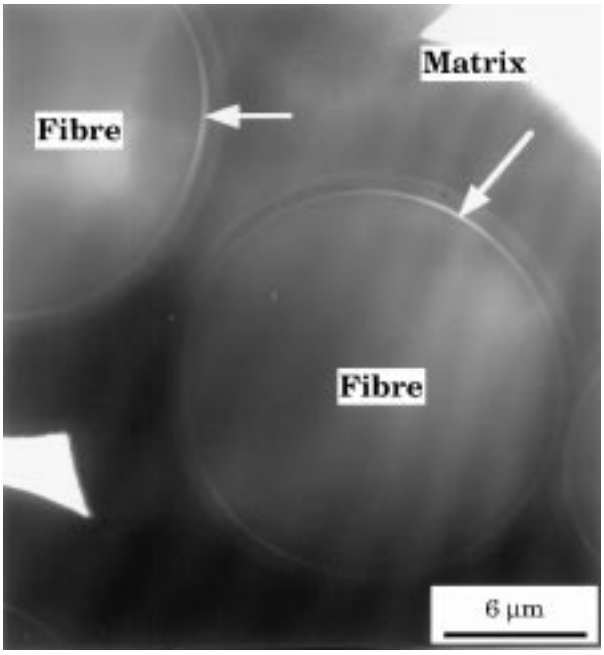

Fig. 15. TEM cross-section of a minicomposite reinforced with a pristine Hi-Nicalon fibre (arrows: debonding due to fibre contraction).

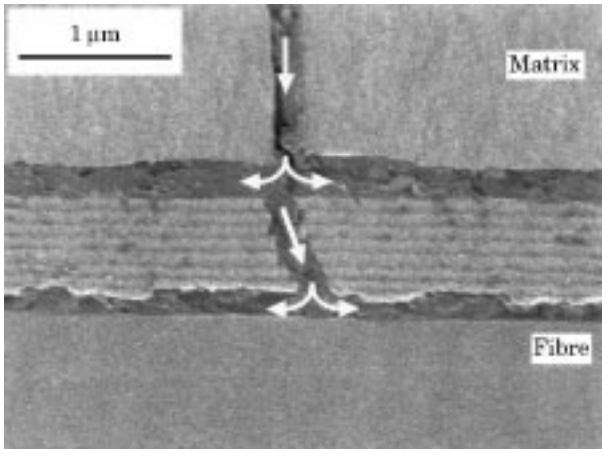

Fig. 16. SEM longitudinal section showing the deflection of a large matrix crack at the fibre surface and at matrix/multilayer interface (non treated Hi-Nicalon reinforced minicomposite) (according to Ref. 20).

result, the interface is effectively weak on most of the fibre surface. The multilayer cannot work. Matrix cracks deflection is systematically occurring at the fibre surface; but also at the matrix/multilayer interface as shown in Fig. 16.

When the fibre has been treated, the CTE mismatch between fibre and matrix is correct. The electron microscopy shows that the chemical bonding is weaker. Despite this weakest bonding the composite behaves in a different manner. The very thin residual matrix cracks are deflected on the many interfaces present in the multilayer (multideflection) as shown in Fig. 17. The microcrack does not propagate through the multilayer as in an homogeneous material. Multideflection is meanwhile not abundant and also, final deflection systematically occurs at the first interface. These latter features when compared to those obtained with the strong interface in Section 3.4 are supposed to be due to a mixed regime (adhesive and cohesive failure of the interphase).

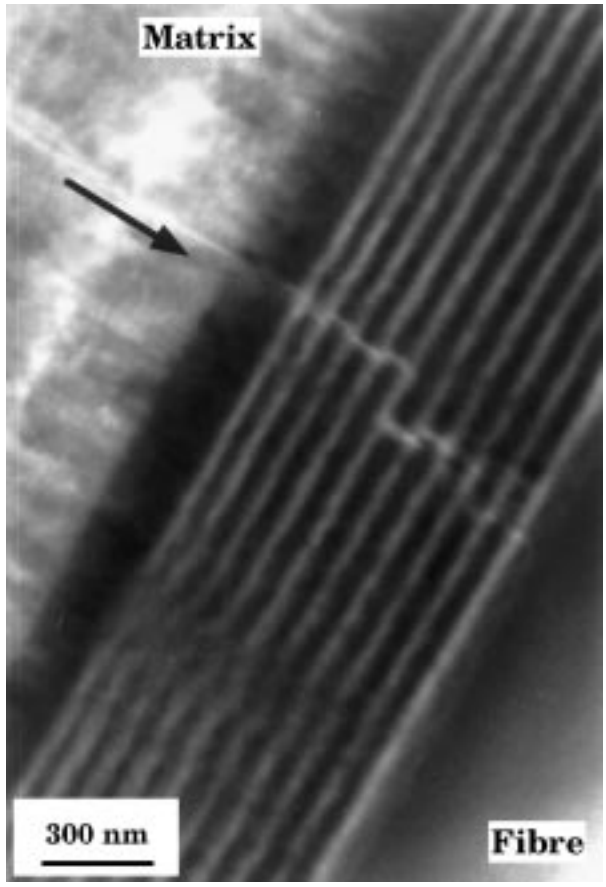

Fig. 17. TEM longitudinal section (treated Hi-Nicalon reinforced minicomposite): multideflection in the PyC/SiC multilayered interfaces.

5. Concluding remarks

This work has compared $(PyC/SiC)_n$ multilayers at two different scales: micrometric scale materials were obtained by I-CVI and nanometric ones by P-CVI. Morphology and behaviour of these two multilayers under mechanical loading, were compared by means of a TEM examination before and after tensile loading test. From the data reported in Sections 3 and 4, several remarks can be drawn.

1. Silicon carbide sublayers morphology obtained by P-CVI are much more homogeneous and

continuous. Only this technique enables to produce multilayers at a nanometric scale, trough a proper control of the residence time and deposition kinetics.

2. Silicon carbide crystallisation is the leading parameter which controls the continuity of the layers and sharpness of the PyC/SiC interfaces. By means of I-CVI, thick layers (0.1 μm) are discontinuous because too much crystallised (scattered nucleation). Conversely, P-CVI was efficient to deposit homogeneous and continuous layers. But pressure cycling does not produce any crystallisation break. CVI parameter and especially MTS/H_2 ratio plays an important role.
3. P-CVI of pyrocarbon allows a close control of the deposit thickness. Both processes produce a pyrocarbon which flattens the roughness of the SiC substrate. Thin sublayers of carbon are efficient to get good mechanical properties.
4. Both types of multilayers (micro and nano) appeared efficient to deflect matrix microcracking in loaded composites at ambient temperature. It has been shown in a previous paper[11] that the multilayer can increase together, strength and toughness in SiC/SiC composites. The only condition is to get some residual radial tensile stress and a strong chemical bonding at the fibre surface. This is the case for treated Nicalon NLM 202.[4] The interface behaves with a cohesive failure mode and the work to fracture is thus increased. On the contrary, the pristine fibres display a too weak bonding and the interface behaves with an adhesive failure mode controling the debond-sliding mechanism.
5. With the pristine Hi-Nicalon fibre, a strong bonding takes place in minicomposites fabricated by P-CVI process, but the important contraction of this fibre[26] brings about an important debonding of most of the fibre surface. This debonding prevents the multilayer to act as mechanical fuse.
6. In the case of treated Hi-Nicalon fibre, the contraction is limited but the treatment leaves a poorly organised carbon at the surface of the fibre. As a result, the bonding strength is too weak. The favourable balance between the residual tensile stress and chemical bonding enables to get an enhanced toughness in this case. This is emphasised in a companion paper.[20]

Acknowledgements

This work has been supported by CNRS and SEP through grants given to S. Bertrand and C. Droillard. The authors wish to thank M. Alrivie, from LCTS and P. Garetta, from CREMEM (University of Bordeaux-1) for their help in TEM samples preparation.

References

1. Evans, A. G., Zok, F. W. and Davis, J., The role of interfaces in fibre-reinforced brittle matrix composites. *Compos. Sci. Technol.*, 1991, **42**(3), 3–24.
2. Naslain, R., Fibre-matrix interphases and interfaces in ceramic–matrix composites processed by CVI. *Composite Interfaces*, 1993, **1**, 253–286.
3. Cao, H. C., Bischoff, E., Sbaizero, O., Ruhle, M., Evans, A. G., Marshall, D. B. and Brennan, J. J., Effect of interfaces on the properties of fibre-reinforced ceramics. *J. Am. Ceram. Soc.*, 1990, **73**(6), 1691–1699.
4. Naslain, R., The design of the fiber-matrix interfacial zone in ceramic matrix composites. *Composites Part A*, 1998, **29A**, 1145–1155.
5. Jacques, S., Guette, A., Langlais, F. and Naslain, R., C(B) materials as interphases in SiC/SiC model microcomposites. *J. Mater. Sci.*, 1997, **32**, 983–988.
6. Boisver, R. P., Hutter, R. K. and Diefendorf, R. J., Interface manipulation in ceramic matrix composites for improved mechanical performance. *Proc. JP, US Conf. Compos. Mater. 4°*, 1989, 789–798.
7. Naslain, R., The concept of layered interphases in SiC/SiC. *Ceram. Trans.*, 1995, **58**, 23–26.
8. Clegg, W. J., The fabrication and failure of laminar ceramic composites. *Acta. Met. Mat.*, 1992, **40**(11), 3085–3093.
9. Folsom, G., Zok, F. W. and Lange, F. F., Flexural properties of brittle multilayer materials: II experiments. *J. Am. Ceram. Soc.*, 1994, **77**(8), 2081–2087.
10. Ignat, M., Nadal, M., Bernard, C., Ducarroir, M. and Teyssandier, F., Mechanical response and rupture modes of SiC/C CVD lamellar composites. *J. Physique, Colloque C5*, 1989, **50**, 259–267.
11. Droillard, C., Lamon, J. and Bourrat, X., Strong interface in CMCs, a condition for efficient multilayered interphases. *Mat. Res. Soc. Proc.*, 1995, **365**, 371–376.
12. Droillard, C. and Lamon, J., Fracture toughness of 2D woven SiC/SiC CVI-composites with multilayered interphases. *J. Am. Ceram. Soc.*, 1996, **79**(4), 849–858.
13. Pasquier, S., Thermomechanical behaviour of SiC/SiC composite with multilayered interphase—effect of the environment. Ph.D. thesis, no. 1727, University of Bordeaux I, France, 1997 (in French).
14. Heurtevent, F., Nanoscale-multilayered $(PYC/SiC)_n$ materials—application as interphases in thermostructural composites. Ph. D. thesis, no. 1476, University of Bordeaux I, France, 1996 (in French).
15. Droillard, C., Bourrat, X. and Naslain, R., Weak and strong interface in ceramic matrix composites: TEM approach of fracture mechanics. *J. Eur. Ceram. Soc.*, in press.
16. Naslain, R. and Langlais, F., CVD-processing of ceramic-ceramic composite materials. In *Tailoring Multiphase and Composite Ceramics*, ed. R. E. Tressler, G. L. Messing, C. G. Pantano and R. E. Newnham. *Mater. Sci. Res.*, Plenum Press, New-York, 1986, pp. 145–164.
17. Naslain, R., Langlais, F. and Fedou, R., The CVI-processing of ceramic matrix composites. *J. de Physique, Colloque C5*, 1989, **50**, 191–207.
18. Naslain, R., CVI-composites. In *Ceramic–Matrix Composites*, ed. R. Warren. Blackie, Glasgow and London, 1992, pp. 199–244.
19. Jouin, J. M., Cotteret, J. and Christin, F., SiC/SiC interphase: case history. In: *Proc. 2nd European Colloquium on Designing Ceramic Interfaces*. CEE Joint Res. Center, Petten (NL), 11–13 November 1991.

20. Bertrand, S., Forio, P., Pailler, R. and Lamon, J., Hi-Nicalon/SiC minicomposites with $(PyC\text{-}SiC)_n$ nanoscale-multilayered interphases. *J. Am. Ceram. Soc.*, in press.
21. Bourrat, X., Trouvat, B., Limousin, G., Vignoles, G. and Doux, F., Pyrocarbon anisotropy as measured by electron diffraction and polarised light. *J. Mater. Sci.*, in press.
22. Dupel, P., Bourrat, X. and Pailler, R., Structure of pyrocarbon infiltrated by pulse-CVI. *Carbon*, 1995, **33**(9), 1193–1204.
23. Lowden, R. A. and More, K. L., The effect of fibre coatings on interfacial shear strength and the mechanical behavior of ceramic composites. *Mater. Res. Soc. Proc.*, 1990, **170**, 205–214.
24. Stinton, D. R, Hembree Jr, D. M., More, K. L., Sheldon, B. W. and Besmann, T. M., Characterization of ceramic matrix composites fabricated by chemical vapor infiltration. In *Chemical Vapor Deposition of Refractory Metals and Ceramics*, ed. T. M. Besmann and B. M. Gallois. Mater. Res. Soc. Symp. Proc., Vol. 168, 1990, 273–280.
25. Schamm, S., Mazel, A., Dorignac, D. and Sevely, J., Observation en microscopic électronique à haute résolution du polytypisme de SiC dans la matrice d'un composite SiC/SiC (HR-TEM observation of SiC polytypes in the matrix of SiC/SiC composite). In *Matériaux Composites pour Applications à Hautes Températures*, ed. J.Lamalle R. Naslain and J. L. Zulian. AMAC-CODEMAC, Paris and Bordeaux (in French), 1990, pp. 207–219.
26. Yun, H. M. and DiCarlo, J. A., High temperature contraction behavior of polymer-derived SiC fibers. In *Ceramic Engineering and Science Proceedings, 21st Annual Conference on Composites, Advanced Ceramics, Materials, and Structures—A*, Vol. 18, Issue 3. The American Ceramic Society, 1997, p. 126.